

Gyrokinetic Edge Turbulence and the Edge/Core Transition

B. Scott (bds@ipp.mpg.de and <http://www.rzg.mpg.de/~bds/>)

Max-Planck-Institut für Plasmaphysik, EURATOM Association, D-85748 Garching, GER

Abstract The gyrokinetic model for low frequency turbulence in magnetised plasmas is applied to the tokamak edge. The transition from the edge region into the core shows clear effect of the changing collisionality and perpendicular/parallel scale length ratios. The results are very similar to corresponding gyrofluid ones, with the exception that the electron population with large perpendicular energy but small parallel velocity behaves much like a separate species even in the absence of trapping effects. This population participates only marginally in the adiabatic response.

1. Overview of Tokamak Edge Turbulence

The experimental situation of the tokamak edge is characterised by moderate collisionality and by steep gradients [1]. The implication for the dynamics of low frequency ExB eddy turbulence in this regime follows from the frequency and scale ratios implicit in several of the dimensionless parameters as discussed below [2]. Observations, where available [3], have always indicated fluctuations in the 10 percent range on closed flux surfaces with relative amplitudes such as $e\tilde{\phi}/T_e$ and \tilde{p}_e/p_e for the electrostatic potential and electron pressure at similar magnitude. Frequencies are broadband and up to what translates to ω values over 1 MHz. The scale of motion as revealed by correlation length measurements is typically about 5 to 10 ion gyroradii [4]. This information together suggests that edge turbulence is fundamentally nonlinear, involving all scales of motion between the drift scale ρ_s and the profile scale L_\perp (here note $\rho_s = \rho_i$ if $T_i = T_e$). One should therefore not be thinking in terms of what mode is causing it, but rather of a broad spectrum covering the entire range of ExB drift dynamics acting as a unit. In other words, drive and saturation and energy transfer mechanisms, rather than an instability.

There are two main things to realise about the qualitative nature of tokamak edge turbulence: it is not an MHD process, and it is not determined by the properties of linear instabilities — neither the drive mechanism nor the parameter scaling. The reason for the nonlinear nature of edge turbulence is the existence of a robust electron density ExB nonlinear advection. This is allowed to exist by the relative strength of the nonlinear perpendicular ExB dynamics in comparison to the (mostly linear) parallel electron dynamics. The following is a summary of the experience from computational models which carry all the relevant scales of motion for edge turbulence (cf. Refs. [2,5] and references therein).

The key parameters are those which reflect this competition: the normalised mass ratio $\hat{\mu} = (m_e/M_i)(qR/L_\perp)^2$, the drift wave collisionality $C = 0.51(\nu_e L_\perp/c_s)\hat{\mu}$, and the drift Alfvén parameter $\hat{\beta} = (4\pi p_e/B^2)(qR/L_\perp)^2$. These give, respectively, the square of the ratio c_s/L_\perp to V_e/qR , the ratio c_s/L_\perp to $(V_e^2/0.51\nu_e)(1/qR)^2$, and the square of the ratio c_s/L_\perp to v_A/qR , hence the relative importance of the drift dynamics (c_s/L_\perp) to either the parallel electron thermal transit (V_e/qR), the resistive diffusion rate, or the Alfvén transit (v_A/qR). For core turbulence all of these except possibly $\hat{\beta}$ are very small, owing to the moderate values of R/L_\perp . For edge turbulence, closer to the location at which the temperature profile would extrapolate to zero, the values of R/L_\perp are in the range of several tens, so that $\hat{\mu} > 1$. This allows the electrons to be nonadiabatic regardless of collisionality, though at these temperatures (of order 100 eV) we always also have $C > 1$ and hence are in the regime of collisional drift waves. However, the ballooning collisionality $\nu_B = C(2L_\perp/R)$ is still below unity. In modern tokamaks the

density is also simultaneously high enough that $\hat{\beta} > 1$, making the response of the electrons electromagnetic as well as nonadiabatic.

These parameters enter because with a sheared magnetic field on closed flux surfaces the parallel gradient is nonzero for every degree of freedom available in the set of variables and wavenumbers. The parallel electron pressure gradient is neither large nor small compared to the parallel electric field. The result is a strong cross coherence and energetic coupling between the electrostatic potential and electron pressure disturbances. An adiabatic response refers to the tendency of the electrons to reach force balance, with parallel gradients of the electron pressure and electrostatic potential in balance, and hence a tendency of these two variables to track each other. This adiabatic response is central to the dynamics but absent in an MHD model.

The reason the turbulence is always nonlinear is more subtle. In linear theory, “diamagnetic effects” due to the largeness of the diamagnetic frequency ω_* compared to the linear growth rate γ_L most often do not change the qualitative nature of the instability — neither for tearing modes nor for ballooning instabilities. The qualitative nature of a ballooning instability refers not to its eigenmode structure but to the process by which the ExB flow disturbance is maintained, in this case by the interchange effect on the low-field side of the torus. However, when the dynamics is both nonlinear and nonadiabatic, the ExB vorticity advection, representing the polarisation current, maintains the parallel current divergence at strong levels, larger than the interchange effect can account for. The interchange effect is lost at short wavelength and the basic mode structure reflects collisional drift (Alfvén) dynamics. This nonlinear instability (“self sustained turbulence” [6,7]) roughly follows ω_* in strength, while γ_L at the same wavenumber is somewhat less than γ_I , the ideal interchange growth rate. In the longer wavelengths, which are not strongly unstable, there remains some ballooning activity, accounting for about 25 percent of the overall turbulent flux, which is nonlinearly maintained by the inverse cascade tendency of the vorticity nonlinearity.

Finally, the remaining main concept is scale separation. We have the importance of the edge turbulence regime $\hat{\mu} > 1$, which requires $qR/L_\perp > 60$. But the regime with $\gamma_I < 0.2\omega_*$, which makes possible a range $0.2 < k_y\rho_s < 1$ in which the self sustained drift wave turbulence can take over, requires R/L_\perp in its realistic range of over 30. At the same time, the range near $k_y\rho_s = 0.2$ occurs where there are still many wavenumbers available in both perpendicular directions. This requires the drift parameter $\delta = \rho_s/L_\perp$ to be in its realistic range of less than 0.02 since the smallest available value of $k_x L_\perp$ for an eddy is π , so that if $\delta = 0.02$ we have $k_x L_\perp = \pi$ for about $k_x\rho_s = 0.06$ and the range $k_\perp L_\perp = 0.1$ still has several degrees of freedom which are allowed to be roughly isotropic, that is, properly turbulent.

It is clear that a model or code which does not open up all of these windows cannot treat edge turbulence because it will be treating something qualitatively different. The spectral ranges won't have enough space to function differently in the longer and shorter wavelengths. The self sustained drift wave regime won't be present at all. And either the range $k_x L_\perp = \pi$ or $k_y\rho_s = 1$ will not have available isotropic degrees of freedom and hence will not function like turbulence. Many of the results in the literature that either neglect or note the absence of drift wave effects already for these reasons make impossible to reach a different conclusion. Even some models which could in principle treat this dynamics properly do not do so because the spectral region near $k_y\rho_s = 1$ is absent for some or all of the cases considered.

2. Desirability of a Kinetic Model

Argument about the kinetic nature of the dynamics has usually centered on the electrons, specifically, long mean free path effects. The resulting modification to the parallel thermal conductivity is what enters. However, the frequency range of the turbulence extends quite close to the collision frequency ν_e and so temporal considerations should also enter. In the electron dynamics these two limits are sufficiently marginal that the effect is not qualitative. With $\omega < \nu_e$ the response of the parallel heat flux to the temperature is still constitutive and long mean free path effects can be captured using a Landau model.

It is the ions that pose a stronger problem for the usual collisional models. With $T_i \sim T_e$ the need to treat ρ_s implies the need to treat unit-order finite gyroradius effects; no expansion-based gyroviscosity model can rescue the situation. Moreover, the ion collision frequency ν_i is very slow. Not only is $\omega \gg \nu_i$, one also has $\omega \gg c_s/qR$, both by about two orders of magnitude. Ion dissipation channels (viscosity, heat flux) are very badly modelled by collisional fluid equations in this situation. Previous work has often done well to avoid ion dissipation entirely, but it is being considered more often, and usually with models which are at least those two orders of magnitude outside their validity. With both of the above inequalities, the situation cannot be saved by “flux limits” since the actual response of the parallel heat flux to the temperature or the parallel viscosity (actually, the temperature anisotropy $\tilde{T}_{i\parallel} - \tilde{T}_{i\perp}$) to flow divergences is no longer constitutive, since the strongest effect in the determination of these diffusive processes is the nonlinear ExB time derivative (turbulent advection). However, it is still possible to capture these effects with a gyrofluid model which treats the turbulent advection in these processes (i.e., they are given their own dynamical equations) [8].

The remaining consideration is velocity space effects in the electrons, specifically, to what extent different regions of velocity space can have completely different dynamics. The clearest case of this is trapped electrons. No gyrofluid model of these can be built in the absence of bounce averaging (recall that ω reaches values larger than V_e/qR) without the correct behaviour being known from a gyrokinetic computation in the context of turbulence. However, although we will find that trapping itself does not have strong effect, we will also find that the region of velocity space with significant energy but small parallel velocity effectively decouples from the rest of the electrons because it does not strongly feel the adiabatic response. Very significant fluctuation anisotropy results, and the extent to which the gyrofluid model can be made to capture this is uncertain.

3. Model Equations

For this study we use the Vlasov method as developed for collisionless drift wave and drift-Alfvén turbulence in Refs. [9,10]. The basic scheme used there was built to handle the parallel electron dynamics for arbitrary values of $k_{\perp}\rho_s$, which is especially critical since the Alfvén response includes both the deep MHD and electrostatic/kinetic limits. The ability to treat the damping of kinetic shear Alfvén waves in these regimes was demonstrated in Ref. [11].

Extension of the model to treat edge turbulence includes incorporation of the appropriate coordinate metric techniques to allow slab-character dynamics [12] as well as a suitable collision operator. We use the space/time discretisation most applicable to wave dynamics and nonlinearities with Poisson bracket structure as used in the gyrofluid GEM code [8], after its original development for the drift fluid model [5]. Spatial bracket structures are given a special discretisation [13]. Trapping is represented by an additional bracket structure, between the parallel space and parallel velocity coordinates, evaluated with a second-order characteristic method [14]. The collision operator is linearised around the

background Maxwellian, and both pitch angle- and energy-scattering components are kept in the standard form developed by Kulsrud [15]. It is given a conservative finite volume discretisation. The linear drive term involving a single first order derivative is done with a standard centered difference. The time stepping is a third-order scheme expanding both the time derivative and combined right hand side across three time steps, evaluating the right hand side only once per time step [16]. It is stable and highly accurate for both waves and bracket nonlinearities.

In terms of these Poisson bracket structures, the additional linear gradient drive, and the collision operator, the delta-f gyrokinetic equation is given by

$$\frac{\partial G}{\partial t} + \delta\omega_T F^M \frac{\partial \psi_e}{\partial y} + [\delta\psi, H]_{xy} + [\delta_a \psi + v_{\parallel} \chi, H]_{xs} - (\mu B) \frac{\chi'}{m} [\log B, f]_{sv_{\parallel}} = C(f) \quad (1)$$

and the self consistent field equations represent polarisation,

$$\sum_{\text{sp}} \int d\mathcal{W} \left[eJ_0 f + e^2 \frac{F^M}{T} (J_0^2 - 1) \phi \right] = 0 \quad (2)$$

and induction,

$$\nabla_{\perp}^2 A_{\parallel} + \frac{4\pi}{c} \sum_{\text{sp}} \int d\mathcal{W} [ev_{\parallel} J_0 f] = 0 \quad (3)$$

with the integrals over velocity space $\int d\mathcal{W} = \int B d\mu dv_{\parallel}$ and the sum over species. This closes the set of dependent variables $f(x, y, s, v_{\parallel}, \mu)$ and ϕ and A_{\parallel} both dependent upon (x, y, s) , with $G = f + e(v_{\parallel}/c)(F^M/T)J_0(A_{\parallel})$ and $H = f + e(F^M/T)J_0(\phi)$, respectively representing the inductive and nonadiabatic responses.

The bracket structures are $[f, g]_{ab} = [(\partial_a f)(\partial_b g) - (\partial_b f)(\partial_a g)]$, and the generalised potentials are $\psi_e = J_0(\phi - [v_{\parallel}/c]A_{\parallel})$ and $\psi = \psi_e + e^{-1}(mv_{\parallel}^2 + \mu B) \log B$, respectively incorporating ExB advection (ϕ), the magnetic flutter nonlinearity (A_{\parallel}), and curvature and grad-B drift effects ($\log B$), where m and e and T and J_0 and the background Maxwellian F^M are set for each species. The sv_{\parallel} -bracket is magnetic trapping. The factor of B is understood as constant except for $\log B$ in the curvature and trapping terms. The drift parameters are $\delta = c/B$ and $\delta_a = c/Ba$, becoming $\delta = \rho_s/L_{\perp}$ and $\delta_a = \rho_s/a$ in normalised units, where a is the minor radius. The term involving ω_T gives the background gradient drive, with $\omega_T = L_n^{-1} + L_T^{-1}(mv^2/2T - 3/2)$, and the quantity $\chi = \chi(x)$ where $\chi' \equiv \partial\chi/\partial x = 1/qR$ gives the ballistic streaming along unperturbed field lines, determining the connection length. The factor of J_0 is the standard gyroaveraging operator. It is applied in \mathbf{k}_{\perp} -space, consistent with the Dirichlet boundaries in x (the half-wave Fourier transform in x is used).

At each time step, G is advanced to $t = t_{n+1}$ knowing the complete information at $t = t_n, t_{n-1}$, and t_{n-2} , and then using G the field equations are solved in \mathbf{k}_{\perp} -space for ϕ and A_{\parallel} and therefore also f and H , using the appropriate manipulations following from the definitions.

The spatial grid is set up as in Ref. [12], capturing the dynamical scale range, respecting global consistency in the parallel wavenumbers [17], and representing the ‘‘thin atmosphere’’ property of the edge so that $L_x \ll L_y$ [2]. The velocity space grid extends to $-5 < z < 5$ and $0 < w < 10$, where T_0 and B_0 are normalising constants and $z = v_{\parallel}/V_{\alpha}$ and $w = \mu B_0/T_0$ are coordinates, with $V_{\alpha}^2 = T_0/m_{\alpha}$ for each species α . The background F^M is set equal for both species, hence $T_i = T_e$. The discretisation is equidistant in all five coordinates. The nominal resolution is $32 \times 128 \times 16 \times 16 \times 8$ for x, y, s, z , and w , respectively. The timestep is $0.02L_{\perp}/c_s$.

4. Results

The energy theorem for this model is derived in a manner similar to the gyrokinetic particle models [18,19]. Not shown herein for space reasons, it is given in Ref. [20]. The components of the energy theorem can be used to diagnose the physical processes in the same manner as in drift fluid and gyrofluid models [2].

The standard case run with this model is $qR/L_T = 100$ and $\beta_e = 10^{-4}$ and $\nu_e L_T/c_s = 1$ and $R/L_T = 30$ and $L_n = 2L_T$ with same $L_T = L_\perp$ for (e, i) and $\delta = 10\delta_a = 0.015$, run into saturation (start amplitude 10^{-4} , linear overshoot at $t = 50$, saturation after 200, run to 1200, with times in units of L_T/c_s here and below).

Selected amplitude ('n' for \tilde{n}_e , 't' for \tilde{T}_e , 'i' for \tilde{T}_i , 'w' for $\tilde{\Omega} = \tilde{n}_e - \tilde{n}_i$, 'p' for $\tilde{\phi}$) and zero-FLR estimated transport ('n' for $\tilde{n}_e \tilde{v}_E^x$, 't' for $0.5\tilde{T}_{e\parallel} \tilde{v}_E^x$, 'i' for $0.5\tilde{T}_{i\parallel} \tilde{v}_E^x$, 'T' for $\tilde{T}_{e\perp} \tilde{v}_E^x$, and 'I' for $\tilde{T}_{i\perp} \tilde{v}_E^x$) spectra are shown in Fig. 1. The magnetic flutter spectrum $M_e = \tilde{q}_{e\parallel} \tilde{b}^x$ (not shown) is small but positive. As in previous electromagnetic gyrofluid (GEM) results [2,21], $\tilde{\Omega}$ is flat out to $k_y \rho_s = 1$, the amplitudes peak at long wavelength, and the transport also at long wavelength but with a significant component coming from the $0.3 < k_y \rho_s < 1$ nonlinear drift wave range where the density of states is higher. The transport spectra appear much as in GEM, except for the difference between the 'T' and 't' curves which in GEM are much more similar. The velocity space structure of the electron and ion ExB energy fluxes are also shown. Here we find the principal anisotropy signal, as the population with $\mu B/T \sim 2$ and $v_\parallel \sim 0$ causes the most transport. This is attributable to a weak adiabatic response for this population. It is not a trapping signature, as a control case run without the trapping effect found the same result. The ions, by contrast, for all of which $v_\parallel/qR \ll c_s/L_\perp$ are relatively isotropic. Both species tend to have inward fluxes for low energies, as found previously [22].

On the other hand, the transport scaling with the drift Alfvén parameter $\hat{\beta}$ is very similar to the GEM result, as shown in Fig. 2. The transport in gyro Bohm units ($c_s \rho_s^2/L_\perp^2$ for fluxes) is insensitive to $\hat{\beta}$ until it begins to rise at about $\hat{\beta} = 3$. The cross correlation and phase shift distributions for \tilde{n}_e versus $\tilde{\phi}$, shown for $\hat{\beta} = 1$ and 5 in Fig. 3, reflect the same transition to ideal ballooning found in GEM. Hence the results concerning the lack of a scaling signature for the L-to-H confinement transition from the fluid and gyrofluid models (cf. Ref. [21]) carry over to the gyrokinetic model. This transition is not explained by local parameter scaling variations, at least not when checked by codes which carry all the relevant scales (cf. also Ref. [5]).

In agreement with the GEM result, radial correlation lengths (not shown) are almost always found in the range $5-7\rho_s$ irrespective of ν_e or β_e , in agreement with observations in the outer quarter of the plasma by radius [4]. When the limits associated with either ideal (β_e) or resistive (ν) ballooning at longer wavelength (lower k_y) are reached, the correlation length in the drift direction increases.

The edge-to-core transition may be represented by a linear temperature profile model, by which $T_e = T_i$ and L_T increase together coreward. The corresponding changes are made in the parameters controlling collisionality and plasma beta. The change in the transport spectra is shown in Fig. 4. The intermediate cases have the narrowest spectra. Here, the parallel dynamics is most constrained while the curvature terms are still relatively small compared to the linear drive and the collisional detrapping is still significant. The change in the parallel envelope structure (not shown) reflects an increasing clarity in the ballooning character as the mode structure becomes more core-ITG like. More study of these phenomena will be forthcoming in the near future.

5. Conclusions

This work describes the first use of the gyrokinetic computational model on tokamak edge turbulence. The results are mostly qualitatively equivalent to those of the corresponding 6-moment gyrofluid model (GEM) of Ref. [8]. The part of the electron population with larger than thermal energy but small parallel velocity, however, acts almost as a separate species, even in the absence of magnetic trapping. This is due to the fact that with $v_{\parallel}/qR < c_s/L_{\perp}$ they mostly avoid the adiabatic response. These electrons produce a thermal flux comparable to that of the ions. The mostly parallel streaming electrons contribute a positive but still small magnetic flutter transport. The transition into the core shows a weakening of the electron drive and transport, with increasing dominance of the more familiar core ∇T_i turbulence characterised by weakly nonadiabatic electrons and a narrower drive spectrum. The resulting spatial inhomogeneity of not only the parameters but also the physical response may have a large role in the as yet unexplained edge pedestal phenomenology.

References

- [1] W. Suttrop et al., Plasma Phys. Controlled Fusion **39**, 2051 (1997).
- [2] B. Scott, Plasma Phys. Controlled Fusion **45**, A385 (2003).
- [3] A. J. Wootton et al., Phys. Fluids B **2**, 2879 (1990).
- [4] G. R. McKee et al., Nucl. Fusion **41**, 1235 (2001).
- [5] V. Naulin, Phys. Plasmas **10**, 4016 (2003).
- [6] B. Scott, Phys. Rev. Lett. **65**, 3289 (1990).
- [7] B. Scott, Phys. Fluids B **4**, 2468 (1992).
- [8] B. Scott, arXiv:physics.plasm-ph/0501124, submitted to Phys. Plasmas (2005).
- [9] F. Jenko and B. D. Scott, Phys. Plasmas **6**, 2418 (1999).
- [10] F. Jenko and B. D. Scott, Phys. Plasmas **6**, 2705 (1999).
- [11] T. Dannert and F. Jenko, Comput. Phys. Comm., in press (2004).
- [12] B. Scott, Phys. Plasmas **8**, 447 (2001).
- [13] A. Arakawa, J. Comput. Phys. **1**, 119 (1966), Repr. vol 135 (1997) 103.
- [14] P. Colella, J. Comput. Phys. **87**, 171 (1990).
- [15] R. M. Kulsrud, Y.-C. Sun, N. K. Winsor, and H. A. Fallon, Phys. Rev. Lett. **31**, 690 (1973).
- [16] G. E. Karniadakis, M. Israeli, and S. A. Orszag, J. Comput. Phys. **97**, 414 (1991).
- [17] B. Scott, Phys. Plasmas **5**, 2334 (1998).
- [18] W. W. Lee and W. M. Tang, Phys. Fluids **31**, 612 (1988).
- [19] J. A. Krommes and G. Hu, Phys. Plasmas **1**, 3211 (1994).
- [20] B. Scott et al., The confluence of edge and core turbulence and zonal flows in tokamaks, in *Proc. of the 20th IAEA Conference Fusion Energy (CD-Rom), Vilamoura, Portugal, Nov 2004*, volume IAEA-CSP-20/CD, pages IAEA-CN-116/TH/7-1, Vienna, 2005, IAEA.
- [21] B. Scott, Phys. Plasmas **7**, 1845 (2000).
- [22] F. Jenko, Phys. Plasmas **7**, 514 (2000).

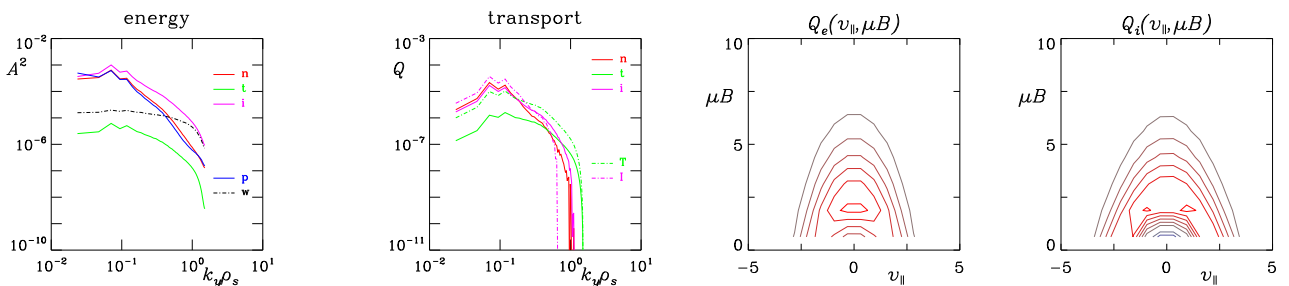


Figure 1: Amplitude and source/sink spectra (left, center left) for the nominal ITG edge case ($\beta_e = 10^{-4}$ and $qR/L_{\perp} = 100$ and $v_e L_{\perp}/c_s = 1$) as explained in the text. Every feature is as found previously in the gyrofluid model, except for the electron temperature anisotropy ('t' versus 'T'). The gyro-Bohm level is 10^{-4} . Velocity space dependence of the electron and ion ExB energy fluxes (center right, right), showing the enhanced role of the electrons with large μB but small v_{\parallel} (thermal velocity units). A control test with the trapping terms removed found the same structure.

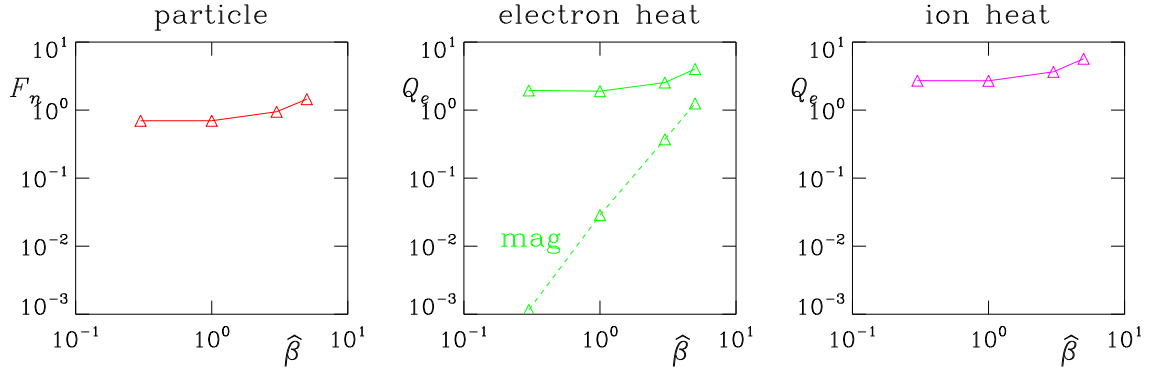


Figure 2: Transport dependence (particle, electron and ion conductive ExB fluxes) upon $\hat{\beta}$, in gyro-Bohm units ($c_s \rho_s^2 / L_\perp^2$ for fluxes). This result is also similar to that from the GEM model.

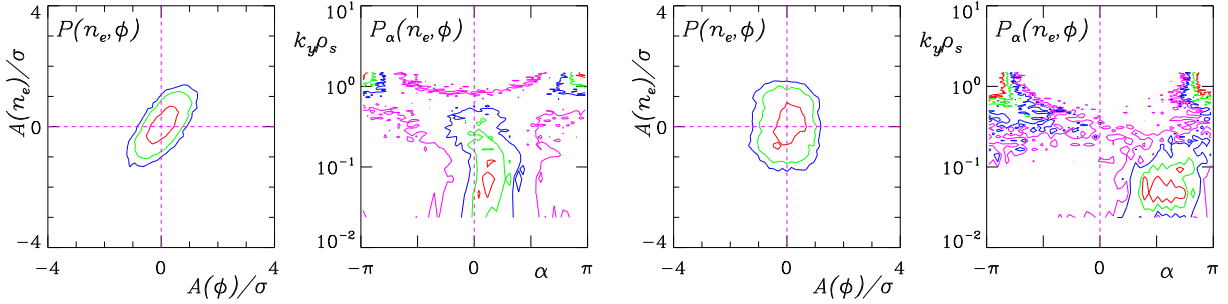


Figure 3: Cross coherence and phase shift distributions for \tilde{n}_e versus $\tilde{\phi}$ in the nominal case $\hat{\beta} = 1$ (left, center left). These are similar to the results from the GEM model. At higher $\hat{\beta} = 5$ the cross coherence is lost and the phase shifts go to $\pi/2$, reflecting the ballooning transition (center right, right).

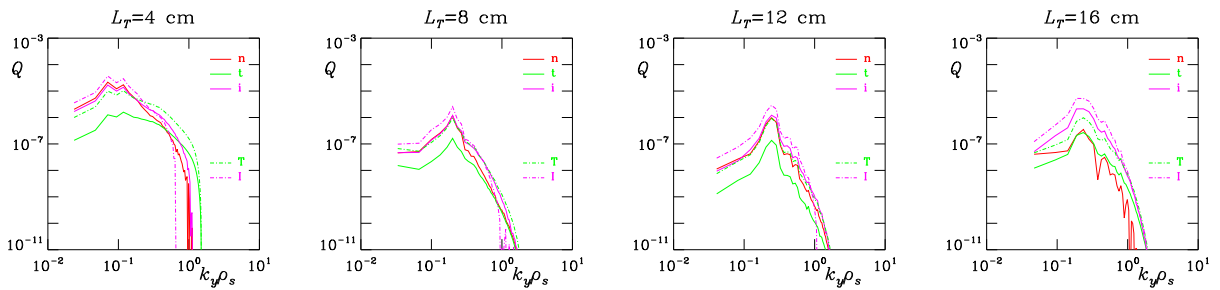


Figure 4: Change in the transport spectra (format as in Fig. 1) from edge to core (left to right) as explained in the text. The gyro-Bohm level is about 10^{-4} . The value of R/L_T drops from 30 to 7.5 in the core.